Journal of Power Sources 196 (2011) 4332–4336

Contents lists available at ScienceDirect

Journal of Power Sources

journal homepage: www.elsevier.com/locate/jpowsour

Short communication

Optimization of $La_{0.6}Ca_{0.4}Fe_{0.8}Ni_{0.2}O_3$–$Ce_{0.8}Sm_{0.2}O_2$ composite cathodes for intermediate-temperature solid oxide fuel cells

N. Ortiz-Vitoriano [a], I. Ruiz de Larramendi [a], J.I. Ruiz de Larramendi [a], M.I. Arriortua [b], T. Rojo [a,*]

[a] Departamento de Química Inorgánica, Facultad de Ciencia y Tecnología, Universidad del País Vasco UPV/EHU, Apdo. 644, 48080 Bilbao, Spain
[b] Departamento de Mineralogía y Petrología, Facultad de Ciencia y Tecnología, Universidad del País Vasco UPV/EHU, Apdo. 644, 48080 Bilbao, Spain

ARTICLE INFO

Article history:
Received 13 June 2010
Received in revised form 26 June 2010
Accepted 25 August 2010

Keywords:
Solid oxide fuel cell
Composite cathodes
Perovskite
Electrochemical impedance spectroscopy

ABSTRACT

Sample of nominal composition $La_{0.6}Ca_{0.4}Fe_{0.8}Ni_{0.2}O_3$ (LCFN) was prepared by liquid mix method. The structure of the polycrystalline powder was analyzed with X-ray powder diffraction data. This compound shows orthorhombic perovskite structure with a space group Pnma. In order to improve the electrochemical performance, Sm-doped ceria (SDC) powder was added to prepare the LCFN–SDC composite cathodes. Electrochemical characteristics of the composites have been investigated for possible application as cathode material for an intermediate-temperature-operating solid oxide fuel cell (IT-SOFC). The polarization resistance was studied using Sm-doped ceria (SDC). Electrochemical impedance spectroscopy measurements of LCFN–SDC/SDC/LCFN–SDC test cell were carried out. These electrochemical experiments were performed at equilibrium from 850 °C to room temperature, under both zero dc current intensity and air. The best value of area-specific resistance (ASR) was for LCFN cathode doped with 10% of SDC (LCFN–SDC9010), 0.13 Ω cm^2 at 850 °C. The dc four-probe measurement exhibits a total electrical conductivity over 100 S cm^{-1} at $T \geq 600$ °C for LCFN–SDC9010 composite cathode.

1. Introduction

Solid oxide fuel cells (SOFCs) are considered one of the most promising energy conversion devices because of their high efficiency, flexibility with respect to fuel and low environmental impact [1,2]. SOFC exploits the high mobility of oxygen ions, O^{2-}, in certain oxides at temperatures higher than 600 °C [3]. Although high temperature SOFCs (HT-SOFCs) have been studied for decades because of their advantages [4], the development of intermediate-temperature SOFCs (IT-SOFCs) is considered to be a realistic approach to accelerate their commercialisation [5]. They are good candidates for stationary power installations and auxiliary power units in trucks [6,7]. Furthermore, lower operating temperatures enable the use of cheaper steels as interconnects [8]. The degradation of stack materials is also reduced and therefore leads to improved reliability and long-term stability. The most common materials for the SOFC are oxide ion conducting yttria-stabilized zirconia (YSZ) for the electrolyte, strontium-doped lanthanum manganite (LSM) for the cathode, nickel/YSZ cerment for the anode, and doped lanthanum chromite or refractory metals as interconnect materials.

One of the main barriers for low-temperature operation is the polarization resistance of cathode [9,10]. Cathodes for SOFC are usually composite cathodes because the requirements are so comprehensive that no single material is able to fulfil them [11]. Creation of composite cathodes is a good way to enhance the cathodic performance. They are composed of a solid electrolyte and an electronic conducting electro-catalytic material. It is widely accepted that composite cathodes, for example $Sm_{0.5}Sr_{0.5}CoO_3$ – Samaria-doped ceria composite cathode (SSC-SDC), can extend the electrochemically active reaction zone from the triple phase boundaries at the two dimensional interface between the electrolyte and the cathode to the three-dimensional bulk of the electrode, and thus improved the cathode performance [12,13]. Furthermore, it is reported that composite cathodes as SSC-SDC, $La_{0.6}Sr_{0.4}Co_{0.2}Fe_{0.8}O_3$ (LSCF)-SDC, and $Ba_{0.5}Sr_{0.5}Co_{0.2}Fe_{0.8}O_3$ (BSCF)-SDC, exhibited rather low interfacial polarization resistance at 600 °C [14,15]. Generally, the composite cathode performance is governed by triple phase boundary (TPB) kinetics, mass transport and ohmic drop [16].

This paper presents a study of the influence on the transport properties of different composite materials $La_{0.6}Ca_{0.4}Fe_{0.8}Ni_{0.2}O_3$ (LCFN) and Samaria-doped ceria (SDC). The electrochemical properties of LCFN/SDC composite cathodes were studied on symmetrical cells employing SDC as electrolyte by varying the relative contents of SDC.

* Corresponding author. Tel.: +34 94 6012458, fax: +34 94 6013500.
E-mail address: teo.rojo@ehu.es (T. Rojo).

0378-7753/$ – see front matter © 2010 Elsevier B.V. All rights reserved.
doi:10.1016/j.jpowsour.2010.08.066

2. Experimental

2.1. Synthesis of electrode

Sample of nominal composition $La_{0.6}Ca_{0.4}Fe_{0.8}Ni_{0.2}O_3$ was prepared by the liquid mix process [17]. Lanthanum nitrate ($La(NO_3)_3$), calcium nitrate ($Ca(NO_3)_2$), iron nitrate ($Fe(NO_3)_3$) and nickel nitrate ($Ni(NO_3)_2$) were used for cathode synthesis ($La_{0.6}Ca_{0.4}Fe_{0.8}Ni_{0.2}O_3$). Stoichiometric amounts of these powders and citric acid were dissolved in distilled water and later a suitable volume of ethylene glycol was added. The resulting solution was agitated and heated in a heating plate until the formation of a gel. After that the gel, which was already treated in a sand bath, was calcined at 600 °C in an oven for 12 h with a 1°/min rate. The sample $La_{0.6}Ca_{0.4}Fe_{0.8}Ni_{0.2}O_3$ is hereafter labelled as LCFN.

In order to improve the electrochemical properties of LCFN cathode, LCFN–SDC composites have been prepared. The ceramic composites LCFN–SDC were obtained from powders synthesized by chemical methods for the cathode, and from commercial powder (Nextech materials) for the electrolyte. The obtained composites with different mass content of SDC: 5, 10, 20, 30, 40, 50 and 60% are named LCFN–SDC9505, LCFN–SDC9010, LCFN–SDC8020, LCFN–SDC7030, LCFN–SDC60-40, LCFN–SDC5050 and LCFN–SDC4060, respectively.

2.2. X-ray characterization

X-ray diffraction (XRD) measurement was carried on a Philips PW1710 and Philips X'Pert-MPD (Bragg-Brentano geometry) diffractometers, with CuKα radiation. XRD pattern was collected with a scanning step 0.001° over the angular range 20–100° with a collection time of 1 h. Structure refinements were fitted using the FullProf software [18]. Graphical representations of XRD patterns were performed using WinPlotr program [19].

2.3. Chemical compatibility

The pairing of oxide ion conducting electrolytes with chemically compatible electrode materials is very important to the performance of SOFCs. In this way, chemical compatibility tests were performed to determinate the interaction between the cathode and the electrolyte. For this purpose, the cathode material and the electrolyte powders were intimately mixed together (weight ratio of 1:1) and isopressed to form a pellet. These pellets were fired at different temperatures for 1 week. Quartz was used as standard material. Then, it was characterized by XRD to investigate the appearance of any reaction products.

2.4. Conductivity measurements of the electrodes

The electrical conductivity of sintered bars of approximate dimensions 1 mm × 3 mm × 7 mm was measured in air from 600 to 850 °C at 50 °C intervals by the Van der Pauw's four-probe technique. Electrical contacts were made using Pt wires and Pt paste placed over whole end faces ensuring a homogeneous current flow. The conductivity (σ) was determined from a set of V–I values by taking $\sigma = 1/\rho = L/A \times dI/dV$, where L is the distance between voltage contacts and A is the sample cross section.

2.5. Area-specific resistance (ASR) from symmetrical measurements

The measurements of electrochemical properties and ASR of the cathodes were performed using a Solartron 1260 Impedance Analyzer. The frequency range was 10^{-2} to 10^{6} Hz with signal amplitude of 50 mV. All these electrochemical experiments were performed at equilibrium from 850 °C to room temperature, under zero dc current intensity and under air over a cycle of heating and cooling. Impedance diagrams were analyzed and fitted using the Zview software. Resistance, capacitance and values of relaxation frequencies were thus obtained by least square refinement.

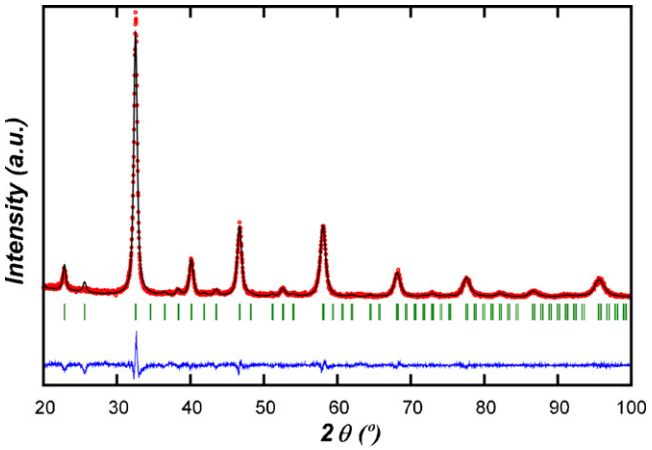

Fig. 1. XRD pattern of $La_{0.6}Ca_{0.4}Fe_{0.8}Ni_{0.2}O_3$ powder obtained by liquid mix method.

3. Results and discussion

3.1. Structural characterization

$La_{0.6}Ca_{0.4}Fe_{0.8}Ni_{0.2}O_3$ was obtained as a pure, well-crystallized single phase, presenting orthorhombic perovskite structure (space group Pnma), similar to those of $LaFeO_3$ [20] and $Ln_{0.6}Ca_{0.4}FeO_3$ [21]. XRD pattern at room temperature for the LCFN sample prepared by liquid mix method is shown in Fig. 1. Calculated cell parameters from XRD data were: $a = 5.5771(6)$ Å, $b = 7.7947(2)$ Å and $c = 5.5027(9)$ Å.

3.2. Chemical compatibility

The reactivity of perovskite materials with most electrolytes which leads to the formation of secondary phases that can affect the electrical conductivity along the cathode/electrolyte interface is an important problem in the use of these materials for SOFC applications [22,23]. Generally, elevated temperatures during processing and fixation of the cell components can lead to chemical reactions between them. An important requirement in SOFCs is the chemical compatibility between cathode material and ionic conductor electrolyte in the composite [24]. For this reason, LCFN sample and SDC electrolyte were mixed together to form a pellet which was sintered at 700, 800 and 900 °C during a week. XRD patterns of the chemical reactivity test are shown in Fig. 2. After calcination at different temperatures, there are no extra diffraction peaks, which may indicate that no significant chemical reaction occur between both materials.

3.3. Electrical conductivity

The electrical conductivities at 600 °C for the LCFN sample with different SDC content in air are shown in Fig. 3. It can be seen that the electrical conductivity remains constant up to 20% SDC content. Then, a further increase in the SDC content leads to a further lowering of the conductivity. The electrical conductivity for LCFN–SDC9010 measured at different temperatures is shown in Fig. 4. The electrical conductivity first increases, reaching a maximum at 750 °C and after that it decreases with increasing temperature. At temperatures lower than 750 °C, where the electrical

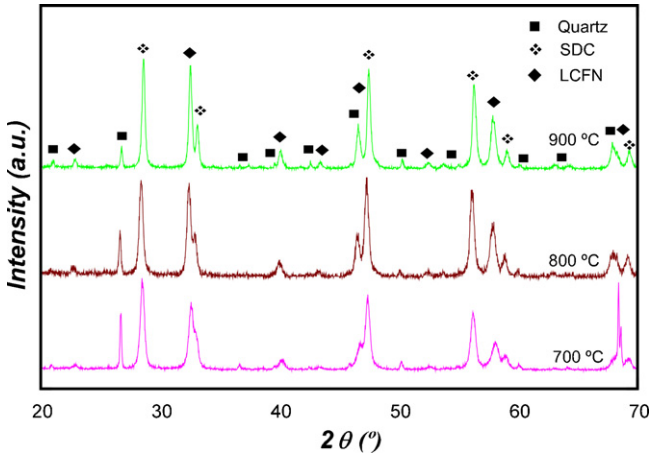

Fig. 2. X-ray diffraction patterns of equimolecular LCFN/SDC mixtures after annealing in air at different temperatures for 1 week.

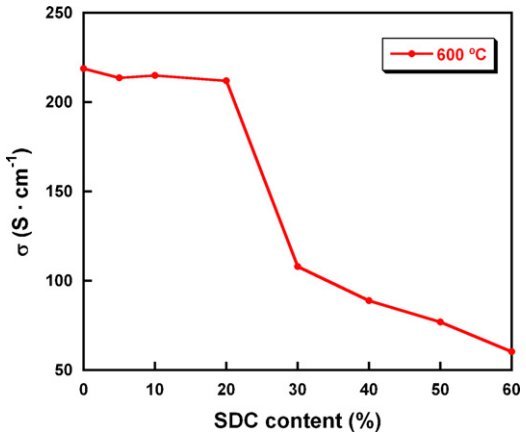

Fig. 3. Arrhenius plot of electronic conductivity of LCFN–SDC composites at 600 °C.

conductivity maximum is observed, a small-polaron semiconducting behaviour is found. The decrease in conductivity after 750 °C could be assigned to the loss of oxygen form the lattice at high temperatures. This result agrees with those described in the literature for other related compounds [25–27]. At low temperatures, the conduction is primarily electronic and is produced by the charge

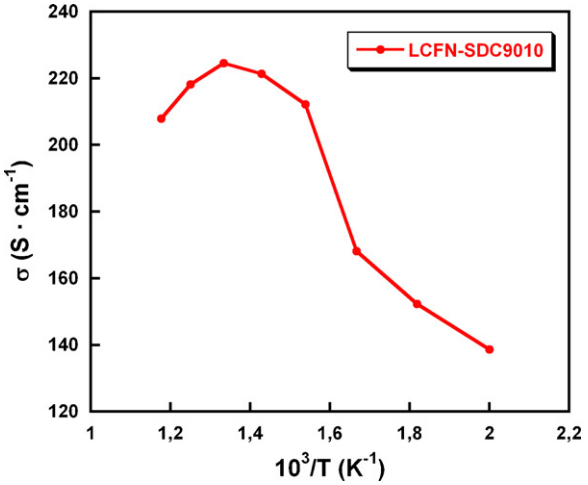

Fig. 4. Arrhenius plot of electronic conductivity of LCFN–SDC9010 composite at different temperatures.

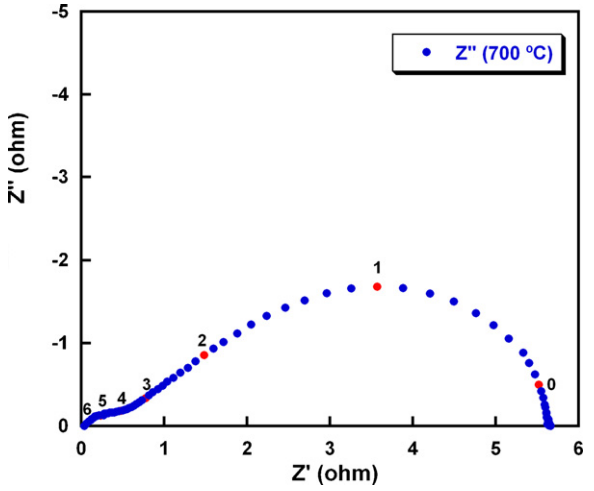

Fig. 5. Impedance pot of LCFN–SDC9010 composite on SDC electrolyte at 700 °C. The numbers in this plot correspond to logarithm of frequency. The impedance data are plotted after electrolyte ohmic drop correction.

compensation, where some Fe cations change from trivalent to tetravalent oxidation state. At higher temperatures, ionic compensation becomes significant as the oxygen content of the material decreases. The LCFN–SDC9010 sample exhibits a conductivity of 215 S cm^{-1} at 600 °C and 225 S cm^{-1} at 750 °C, similar to those reported in the literature [28]. Furthermore, on having doped the LCFN sample with SDC, a drop in the electrical conductivity respect to that $La_{0.6}Ca_{0.4}Fe_{0.8}Ni_{0.2}O_3$ (219 S cm^{-1}) is obtained. This fact can be explained by the introduction of an ionic conductor (SDC) in LCFN sample.

3.4. Area-specific resistance (ASR) from symmetrical measurements

Several strategies have provided promising results in the performance of these devices, but the knowledge of the processes taking part in SOFC electrodes is partially understood, which makes more difficult the optimization of materials that present degradation problems at short and long term. Its operation varies strongly with many variables that are still unknown and their understanding is limited as to how material properties and microstructure are related to the operation and long-term stability. Electrochemical impedance spectroscopy is a useful technique to clarify the different processes that take place in these devices.

The impedance spectra of LCFN–SDC9010 on SDC electrolyte pellet at 700 °C is shown in Fig. 5. Fig. 6 shows the variation in impedance spectra of LCFN sample and LCFN–SDC9010 composite at 800 °C. In both cases, the impedance response at high

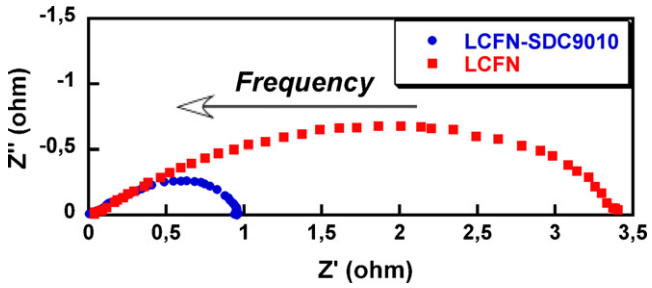

Fig. 6. Impedance pot of LCFN–SDC9010 composite and LCFN phase on SDC electrolyte at 800 °C. The impedance data are plotted after electrolyte ohmic drop correction.

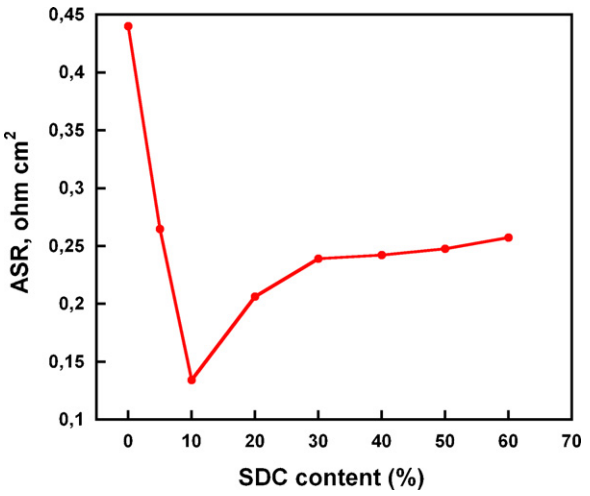

Fig. 7. Arrhenius plots of ASR LCFN–SDC electrodes with SDC electrolyte at 850 °C.

temperatures consists of overlapped semicircles. To carry out the study of the different processes that occur at the electrode, it is important to take into account the different semicircles involved. At high frequencies, a smaller semicircle attributed to charge transfer followed by the ion incorporation into the electrolyte is observed. This contribution is related to the interface and not to the electrode surface. The charge transfer models describe interfacial resistance as a function of the electronic and ionic transport within the two components and the morphology of these components [29]. Other models have been used to describe the interfacial resistance primarily in terms of the internal porosity and the kinetics of oxygen diffusion and surface exchange in the composite material [30]. Both models provide insights into the parameters that influence the performance of composite electrodes. At lower frequencies, a higher semicircle attributed to the oxygen diffusion through the electrode is observed. As can be seen, this semicircle is larger and provides a greater contribution to the total resistance of the electrode. It is possible to compare the obtained impedance spectra for the composites and LCFN sample (Fig. 6) [31]. At high frequencies, the semicircle hardly varies. In contrast, the semicircle at low frequencies is considerably reduced by introducing a 10% of SDC in LCFN sample (LCFN–SDC9010). This result confirms that the diffusion of oxide ions generated in the material surface occurs more easily when SDC is introduced as an ionic conductor mixed with LCFN phase. Another way to confirm these processes is associating capacitance values to each semicircle. Conducting this study has been observed that semicircles at high frequencies present capacitance values of 10^{-6} F while those observed at low frequencies present capacitance values of 10^{-3} F. These results are in good agreement with those described in the literature [32].

The EIS data were used to derive the area-specific resistance (ASR) for LCFN–SDC electrodes. The cathodic area-specific resistance (ASR) is deduced from the relation: ASR = $R_{electrode}$·surface/2. Fig. 7 shows the ASR values at 850 °C as a function of SDC content. With increasing SDC content, a drop of the ASR value is observed up to 10% SDC. Then, the ASR values increase up to 60% SDC. As can be observed, as SDC is introduced, the ionic conductivity provided by the SDC itself adds to the electronic conductivity provided by LCFN. From 20% the resistance value begins to increase, decreasing the electronic conductivity from 210 to 160 S cm^{-1}, approximately. At this point, the contact between the gas and the electrode surface is limited, which difficulties the reactions of adsorption and dissociation of oxygen. Therefore, oxide ions are formed in smaller quantities. Although increasing the amount of ionic conductor if the regions of 2 PB (gas/electrode) are reduced, this will be the limiting factor of conductivity, thus increasing the ASR values.

Therefore, LCFN–SDC9010 cathode presents the better performance in electrochemical measurements, showing an ASR value of 0.13 Ω cm^2 at 850 °C. The original cathode, with an ASR value of 0.44 Ω cm^2, has been improved significantly.

4. Conclusions

$La_{0.6}Ca_{0.4}Fe_{0.8}Ni_{0.2}O_3$ was successfully synthesized by liquid mixed method after calcination at temperature of 600 °C. The crystalline analysis showed that LCFN sample had orthorhombic symmetry with Pnma space group. In order to improve the electrochemical properties of LCFN cathode, LCFN–SDC composites have been prepared. The electrochemical properties of composites cathodes are reported. The best electrochemical performance is for LCFN–SDC9010, exhibiting an ASR value of 0.13 Ω cm^2 at 850 °C. The electrical conductivity of LCFN–SDC9010 composite at temperatures above 600 °C is over 100 S cm^{-1}. These results suggest that the LCFN and SDC composites are promising cathode materials for intermediate-temperature-operation solid oxide fuel cells (IT-SOFC) applications.

Acknowledgements

This work has been partially financed by the Spanish CiCyT under project MAT2007-66737-C02-01 and by the Government of the Basque Country under project IT-312-07. N. Ortiz-Vitoriano thanks the Eusko Jaurlaritza/Gobierno Vasco for her predoctoral fellowship. I. Ruiz de Larramendi thanks the Government of the Basque Country for funding her research activities as postdoc within the Project GIC07/126-IT-312-07.

References

[1] C. Zhu, X. Liu, D. Xu, D. Wang, D. Yan, L. Pei, J. Power Sources 185 (2008) 212–216.
[2] R. Chiba, H. Orui, T. Komatsu, Y. Tabata, K. Nozawa, M. Arakawa, K. Sato, H. Arai, J. Electrochem. Soc. 155 (6) (2008) B575–B580.
[3] I. Ruiz de Larramendi, D.G. Lamas, M.D. Cabezas, J.I. Ruiz de Larramendi, N.E. Walsöe de Reca, T. Rojo, J. Power Sources 193 (2009) 774–778.
[4] B.C.H. Steele, Nature 400 (1999) 619–621.
[5] G. Xiao, Z. Jiang, H. Li, C. Xia, L. Chen, Fuel Cells 09 (2009) 650–656.
[6] T. Norby, Nature 410 (2001) 877–879.
[7] J.I. Ruiz de Larramendi, L. Fidalgo, I. de Meatza, P. Nunez, J.C. Ruiz-Morales, M.I. Arriortua, T. Rojo, Int. J. Mater. Prod. Technol. 27 (2006) 91–100.
[8] K. Huang, P.Y. Hou, J.B. Goodenough, Solid State Ionics 129 (2000) 237–250.
[9] Z.P. Shao, S.M. Haile, Nature 431 (2004) 170–173.
[10] N.P. Brandon, S. Skinner, B.C.H. Steele, Annu. Rev. Mater. Res. 33 (2003) 183–213.
[11] M. Mogensen, S. Primdahl, M.J. Jørgensen, C. Bagger, J. Electroceram. 5 (2) (2000) 141–152.
[12] M.J. Jørgensen, S. Primdahl, M. Mogensen, Electrochim. Acta 44 (1999) 4195–4201.
[13] E.P. Murray, S.A. Barnett, Solid State Ionics 143 (2001) 265–273.
[14] V. Dusastre, J.A. Kilner, Solid State Ionics 126 (1999) 163–174.
[15] K. Wang, R. Ran, W. Zhou, H. Gu, Z. Shao, J. Ahn, J. Power Sources 179 (2008) 60–68.
[16] J. Deseure, Y. Bultel, L. Dessemond, E. Siebert, P. Ozil, J. Appl. Electrochem. 37 (2007) 129–136.
[17] N. Ortiz-Vitoriano, I. Ruiz de Larramendi, I. Gil de Muro, J.I. Ruiz de Larramendi, T. Rojo, Mater. Res. Bull. 45 (2010) 1513–1519.
[18] J. Rodriguez-Carvajal, Physica B 192 (1993) 55–69.
[19] J. Rodriguez-Carvajal, T. Roisnel, FullProf.98 and WinPLOTR: New Windows 95/NT Applications for Diffraction, Newsletter no. 20, May–August, Summer, 1998.
[20] A. Jones, M.S. Islam, J. Phys. Chem. C 112 (2008) 4455–4462.
[21] Y.H. Chen, Y.J. Wei, H.H. Zhong, J.F. Gao, X.Q. Liu, G.Y. Meng, Ceram. Int. 33 (2007) 1237–1241.
[22] H. Taimatsu, K. Wada, H. Kaneko, H. Yamamura, J. Am. Ceram. Soc. 75 (2) (1992) 401–405.
[23] V. Gil, J. Tartaj, C. Moure, J. Eur. Ceram. Soc. 29 (9) (2009) 1763–1770.
[24] G. Zhu, X. Fang, C. Xia, X. Liu, Ceram. Int. 31 (2005) 115–119.
[25] J.W. Stevenson, T.R. Armstrong, R.D. Carneim, L.R. Pederson, W.J. Weber, J. Electrochem. Soc. 143 (9) (1996) 2722–2729.

[26] T. Montini, M. Bevilacqua, E. Fonda, M.F. Casula, S. Lee, C. Tavagnacco, R.J. Gorte, P. Fornasiero, Chem. Mater. 21 (2009) 1768–1774.
[27] X. Zhou, P. Wang, L. Liu, K. Sun, Z. Gao, N. Zhang, J. Power Sources 191 (2009) 377–383.
[28] J.H. Kim, M. Cassidy, J.T. Irvine, J. Bae, Chem. Mater. 22 (2010) 883–892.
[29] C.W. Tanner, K.Z. Fung, A.V. Virkar, J. Electrochem. Soc. 144 (1997) 21–30.
[30] B.C.H. Steele, K.M. Hori, S. Uchino, Solid State Ionics 135 (2000) 445–450.
[31] N. Ortiz-Vitoriano, I. Ruiz de Larramendi, J.I. Ruiz de Larramendi, M.I. Arriortua, T. Rojo, J. Power Sources 192 (2009) 63–69.
[32] Z. Jiang, Z. Lei, B. Ding, C. Xia, F. Zhao, F. Chen, Int. J. Hydrogen Energ. 35 (2010) 8322–8330.